



Failure Analysis of Bearings of Aero-Engine

Manish Roy

Submitted: 12 April 2019 / in revised form: 28 August 2019 / Published online: 21 October 2019
© ASM International 2019

Abstract Failed bearings of various aero-engines were subjected to investigations. The bearing of cooling turbine of aircraft designated as B-1 was found to fail due primarily to misalignment and overloading. Bulk fatigue and permanent dimensional changes also accelerated the failure. The center main bearing of another aero-engine designated as CMB-1 was found nonfunctional because of ‘Brinelling’ action. Lack of lubrication caused over heat and deformation of rollers by metal to metal contact, and this resulted in formation of untempered martensite, leading to failure of center main bearings referred as CMB-2 of another helicopter engine. Stationary race and rotating race of thrust bearing of positive displacement reciprocating hydraulic pump bearing denoted as EDP-1 failed by abrasive action of foreign particles and oxidized metallic particles. In contrast, balls of the same bearing failed because of abrasive action of oxidized metal debris and rolling contact fatigue.

Keywords Contact fatigue · Brinelling · Misalignment · Over heating

Introduction

Bearings are extensively used components in any engineering assembly with diverse applications ranging from domestic (fans, turn tables, etc.) to aerospace. Depending on area of applications, bearings are subjected to radial loading or thrust loading or combination of both types of

loading. Based on operating condition, these bearings are subjected to mechanical or chemical degradation.

Bearings are used in various parts of the aero-engines. Bearings can fail due to several reasons such as contact fatigue, denting, wear, corrosion, misalignment, contamination, etc. [1–4]. A large number of literatures on failures of bearings are available [5–8]. Mishra et al. [5] analyzed the failure of an inter-shaft bearing in an aero gas turbine engine. They attributed the failure to insufficient clearance due to differential expansion of inner ring and contraction of outer ring due to heating and cooling, leading to progressive fatigue as a result of overload. Analysis due to Ejaz et al. [6] indicated that an aero-engine failed due to the misalignment of the ball bearing fitted on the main shaft of the engine. As reported by Bhat et al. [7], ball bearing belonging to jet engine of a military aircraft failed due to eccentricity caused by improper mounting of the bearing onto the shaft of the bevel gear. According to Yu and Yang [8] interaction between dry friction and impact both led outer ring of a cylindrical roller bearing within an air blower motor. Failures of several bearings of aero-engine have been investigated in author’s laboratory over past few years. Results of such investigation have been compiled in this work.

Background

The present article is concerned with failure of several bearings of aero-engine. The bearing of cooling turbine of a fighter aircraft was found dry and damaged. The cage of the bearing was found broken into pieces, and the roller was dislodged from the cage. This bearing is designated as B-1. The center main bearing of another aero-engine used for training purposes designated as CMB-1 was found

M. Roy (✉)
Defence Metallurgical Research Laboratory, Kanchanbagh,
Hyderabad 500058, India
e-mail: rmanish64@rediffmail.com

nonfunctional after attaining dry condition. Similarly the cage was damaged with dislodged rollers. This engine was operated for 975 h. During the strip examination of a helicopter engine, one of the bearings was found failed and the rollers were worn out to approximately 2/3rd of the original diameter and totally deformed. This bearing is referred as CMB-2. Various parts such as balls and races of thrust bearing of positive displacement reciprocating hydraulic pump known as engine-driven pump (EDP) were found badly damaged after operation of 3001.5 h. This resulted in dropping of main hydraulic pressure a low value, against the required delivery pressure when the pump ran at an rpm of 4000. The strip examination of the bearing assembly revealed that the races of the bearing were damaged and the balls were worn out to approximately three fourth of the original diameter. This bearing, hence forth will be termed as EDP-1.

Investigation and Results

Visual Examination

The failed components of B-1 in the as-received condition are shown in Fig. 1a. The inner surface of the outer race indicates the presence of wearing marks due to rubbing by bearing. The inner races were welded with the shaft and damaged completely. Bearing balls were rubbed badly and got damaged. Cage was broken and destroyed totally. The damaged parts of CMB-1 in the as-received condition are provided in Fig. 1b and c. The outer surface of the inner race indicates the presence of marks due to indentation by rollers. The inner surfaces of outer race were also rubbed extensively. Rollers were rubbed and worn out badly. Cage was broken and highly damaged. Figure 1d represents defective parts of CMB-2 in the as-received condition. The outer surface of the inner race and the inner surface of outer race were worn out showing rubbed features. Both races were completely darkened. Rollers were deformed badly and found to lose their original shape. Cage was broken, twisted and damaged. Part of the cage was welded to the inner surface of the outer race. Finally, the damaged components of the thrust bearing (EDP-1) in the as-received condition are shown in Fig. 1e and f. The inner surface of the stationary race (tight ring) and the inner surface of the rotating race (free ring) were heavily rubbed. Balls were rubbed and deformed badly. No apparent damage of the cage is noticed. It is also to be noted that outer surface has not been damaged.

Stereographic Examination

Images of outer race and cage of as-received B-1 obtained from stereo microscopy are also illustrated in Fig. 2a and b. This image also supports damage of components by excessive wear. The races exhibit off center damage from misalignment. The cage shows marks due to scoring, scuffing and plastic deformation. Observation confirming similarity between stereo microscopic image and image of as-received sample of CNB-1 supporting indentation by roller on the outer surface of inner race is presented in Fig. 2c. Stereo microscopic images of outer race and inner race of damaged CMB-2 are given in Fig. 2d and e. These images are also in conformity with images of Fig. 1d. Images of stationary race (tight ring), rotating race (free ring) and ball obtained by stereo microscopy of the EDP-1 bearing are shown in Fig. 2f, g, and h. Highly deformed and uneven surfaces are evident. Careful examination of the ball indicates the presence of surface cracks.

Metallography

Sections of the failed components were prepared for metallographic examination and observed under optical microscope. The microstructures of the races of all three bearings (B-1, CMB-1 and CMB-2) were seen on longitudinal directions. In the case of rollers, the most deformed samples were taken for microstructural examinations. Cages were also mounted on two different directions. In the case of stationary race (tight ring) and rotating race (free ring) of EDP-1 bearing, the microstructure was seen in axial and radial directions. In the case of balls, the most deformed samples were taken for microstructural examinations. The etching reagent used was 2% nital for races, rollers and for cage. The cages which were made of Cu-base alloy of B1 and EDP-1 bearing were etched with acidified potassium dichromate solution.

In the unetched condition, a few oxide inclusions were seen in roller, inner race and outer race. Microstructures of inner races, outer races and rollers or balls of various bearings are provided in Figs. 3, 4 and 5, respectively. Microstructure of the shaft of bearing B-1 exhibits ferritic with equiaxed grains (Fig. 3a). Both inner race and outer race of other bearings show tempered martensitic structure with undissolved carbides as shown in Figs. 3 and 4. The microstructures of the balls and rollers also show undissolved carbides with tempered martensite as shown in Fig. 5. The microstructure of the ball of EDP-1 also exhibited tempered martensite. In the case of the cage (Fig. 6), the microstructure of B-1 consisted dendrites of primary α and transformed β in interdendritic region (Fig. 6a). Cage of CMB-1 shows re-precipitated carbides in a matrix of tempered martensite (Fig. 6b). The

Fig. 1 Photographs of the failed components of various bearings in as-received condition: (a) bearing B-1, (b) bearing CMB-1, (c) bearing CMB-1, (d) bearing CMB-2, (e) EDP-1 and (f) EDP-1



microstructure of the cage of CMB-2 consisted of dendrites of primary α and transformed β in interdendritic region (Fig. 6d). The cage microstructure of EDP-1 revealed dendrites of primary α and transformed β in interdendritic region on etching with acidified potassium dichromate solution.

Chemical Analysis

Elemental analysis of the test materials was done using x-ray fluorescence spectroscopy (XRF) and inductively coupled plasma optical emission spectrophotometer (ICP-OES). Interstitial elements were detected by LECO oxygen and nitrogen analyser. The measured compositions of the investigated materials are given in Tables 1, 2, 3, and 4. It is clear that all parts of and CMB-1 are iron based. In contrast, the cages of B-1, CMB-2 and EDP-1 are Cu–Al bronze. All iron-based components except shaft of B1 and cage of CMB-1 contain carbon close to 1%. Based on microstructure and composition, it can be inferred that the shaft of B-1 is high carbon ferritic stainless steel.

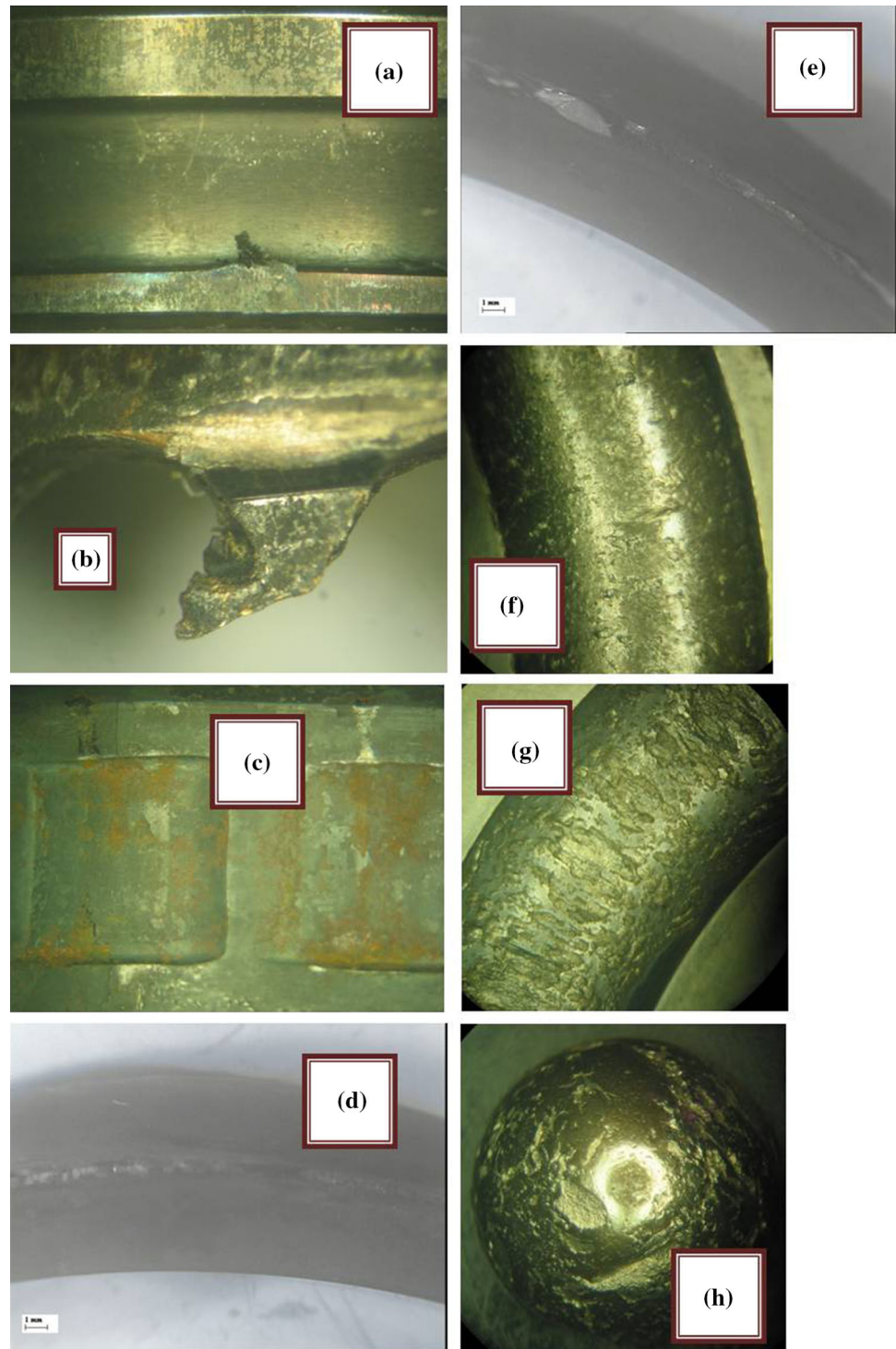
Hardness

Bulk hardness was measured on the roller/the sectioned surfaces of balls, inner race, outer race and cage of main bearings in Vickers scale. Hardness in Vickers scale was also determined for the stationary and rotating races of EDP-1 and the shaft of B1. For roller and race samples, 50 kg load was used while for the cage sample 20 kg load was used. The average values of hardness are given in Table 5. Hardness was found uniform across various locations of various components of the bearing assembly. However, variation was quite large on inner races of CMB-1.

Examination of Damaged Surfaces

Thermal imaging of the shaft and one outer race of bearing B-1 was carried out. Thermal image obtained immediately after flash heating is presented in Fig. 7. Minor stress concentration in some places of the race can be noticed. However, shaft appears to be completely stress free. Image

Fig. 2 Stereo microscopic images of (a) inner race of CMB-1, (b) cage of CMB-1, (c) inner race of CMB-1, (d) outer race of CMB-2, (e) inner race of CMB-2, (f) stationary race (tight ring) of EDP-1, (g) rotating race (free ring) of EDP-1 and (h) balls of EDP-1



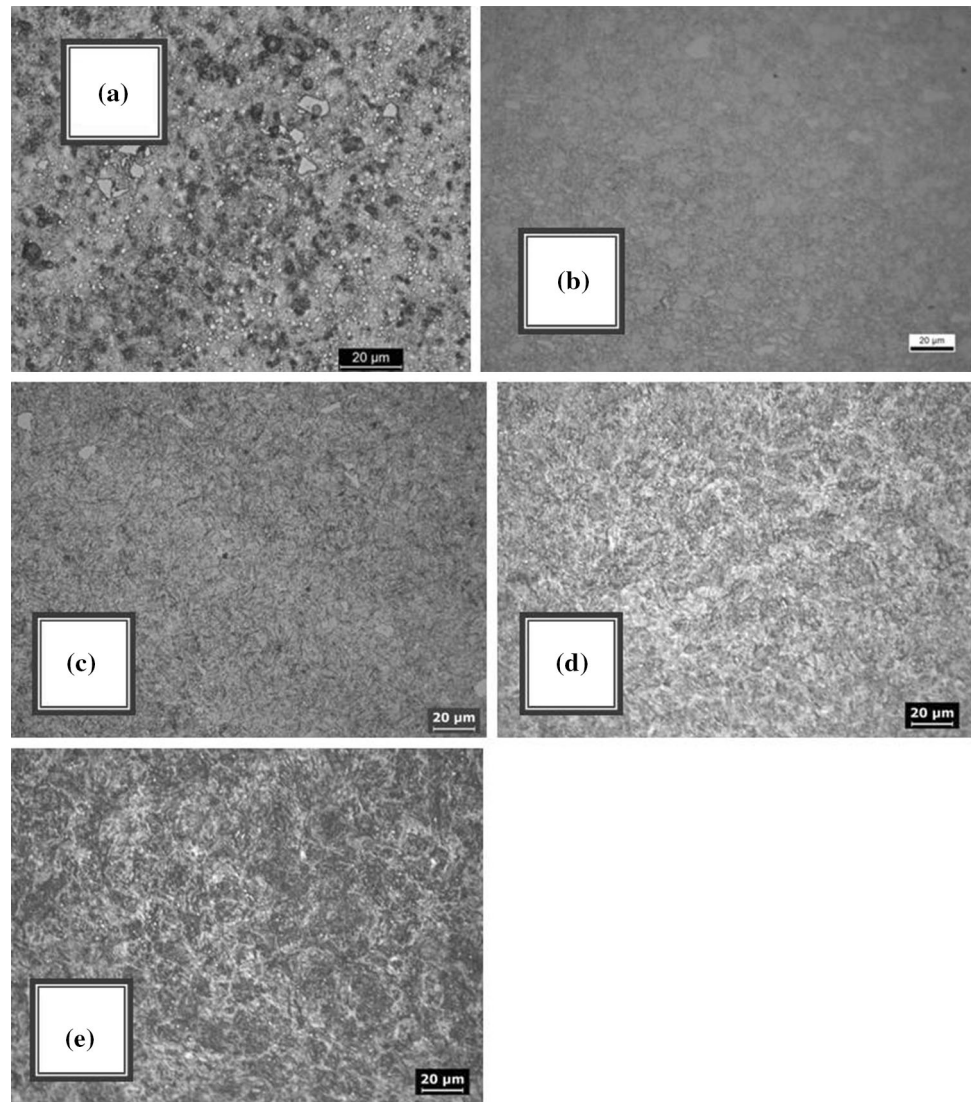
of the shaft obtained after radiography is shown in Fig. 8. A completely defect-free component is evident.

Thermal imaging of the race of CMB-1 was carried out and is presented in Fig. 9. Thermal image of the race is shown immediately after flash heating (Fig. 9a), 15 s after flash heating (Fig. 9b) and 30 s after flash heating

(Fig. 9c). Stress concentration in some places of the race can be noticed.

The high-magnification images obtained by scanning electron microscopy (SEM) of the damaged surface of outer race of CMB-2 along with spectra obtained by energy dispersive spectroscopy (EDS) are presented in Fig. 10a. Extensive plastic deformation of the damaged surface is

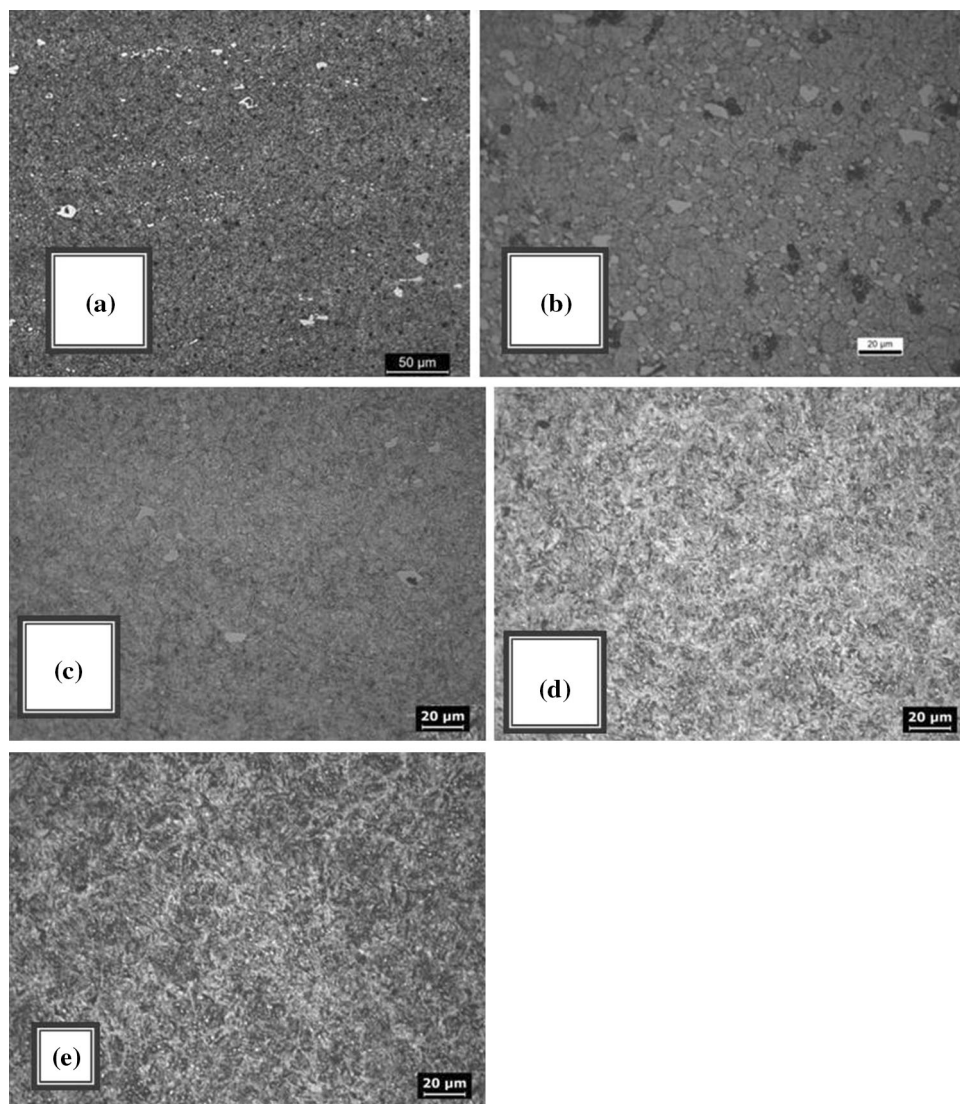
Fig. 3 Optical micrographs of the (a) shaft of B-1, (b) inner race of CMB-1, (c) inner race of CMB-2, (d) stationary race (tight ring) of EDP-1 axial and (e) stationary race (tight ring) of EDP-1 radial



evident [9–11]. The presence of delamination crack can clearly be seen on the worn surfaces [12, 13]. Significant amount of debris can be noted on the inner surface of outer race. The SEM images of the damaged surface of the inner race are given in Fig. 10b. Portion of rubbed surface is covered with oxide scale (Cr_2O_3). Damaged surface of the cylinder shows severely deformed surface and the presence of crack and oxide scale (Fig. 10c). The morphology of damaged surface and the corresponding EDS pattern of the cage are presented in Fig. 10d. Significant oxidation of outer race and inner race is evident. The compositions of these two races obtained by EDS of SEM are close to the measured composition obtained by fluorescence and optical emission spectroscopic analysis. The composition of cage shows the presence of several other elements indicating transfer of materials from the races on the damaged portion along with oxidation [12, 13].

The high-magnification images obtained by scanning electron microscopy (SEM) of the damaged surface of stationary race (tight ring) and rotating race (free ring) of EDP-1 bearing along with spectra obtained by energy dispersive spectroscopy (EDS) are presented in Fig. 11a and b. The presence of extensive plastic deformation characterized by delamination/crack can clearly be seen on the damaged surfaces. In addition, crack due to fatigue can also be observed. The composition obtained by EDS for the main alloying elements from the damaged surface is summarized in Table 6. Clearly, the composition is close to the measured composition obtained by fluorescence and optical emission spectroscopic analysis indicating negligible oxidation, homogeneity of the composition even in the damaged portion and the absence of any transfer layer on the damaged portion. Significant amount of debris can be noted on the rotating race (free ring). SEM micrographs of debris on the rotating race (free ring) along with EDS

Fig. 4 Optical micrographs of the (a) outer race of B-1, (b) outer race of CMB-1, (c) outer race of CMB-2, (d) rotating race (free ring) of EDP-1 axial and (e) rotating race (free ring) of EDP-1 radial



spectra are illustrated in Fig. 11c. In addition to increased amount of oxygen, the presence of foreign element Si can be noticed on the damaged surfaces. SEM images of the damaged surfaces of the ball along with EDS spectra are provided in Fig. 11d. Again severely deformed surfaces and the presence of extensive cracking can be noted. The damaged surface exhibits features of shear dimple and ductile fracture. EDS from debris of the ball did not show the presence of any foreign element although higher wt percentage of oxygen is noted. Optical micrograph of the transverse section of the stationary race (tight ring) is given in Fig. 12. Subsurface crack can be seen in the damaged portion. It can also be seen that some cracks lie completely below the surface, indicating that the crack is generated beneath the surface. However, no crack perpendicular to the surface can be noted. Optical micrograph of the transverse section of the ball is given in Fig. 13. Interestingly subsurface cracks show the presence of delamination

cracks (cracks parallel to the surface) and cracks perpendicular to the surface.

Discussion

Chemical analysis, microstructural studies and hardness suggested that the race and roller of bearing nearly confirmed to hot working tool steel as per the ASTM specification and were used in the hardened and tempered conditions. Chemical analysis of the cage showed that it was made of Cu–Al brass except for CMB-1. The cage of CMB-1 was made of 52,100 steel and used in tempered martensite condition. However, the microstructure and the hardness suggested that the cage made of Cu–Al brass was used in the as cast condition. The shaft of bearing B-1 was made of ferritic stainless steel. The microstructural features and the composition are uniform throughout various parts

Fig. 5 Optical micrographs of the (a) ball of B-1, (b) roller of CMB-1, (c) roller of CMB-2 and (d) ball of EDP-1

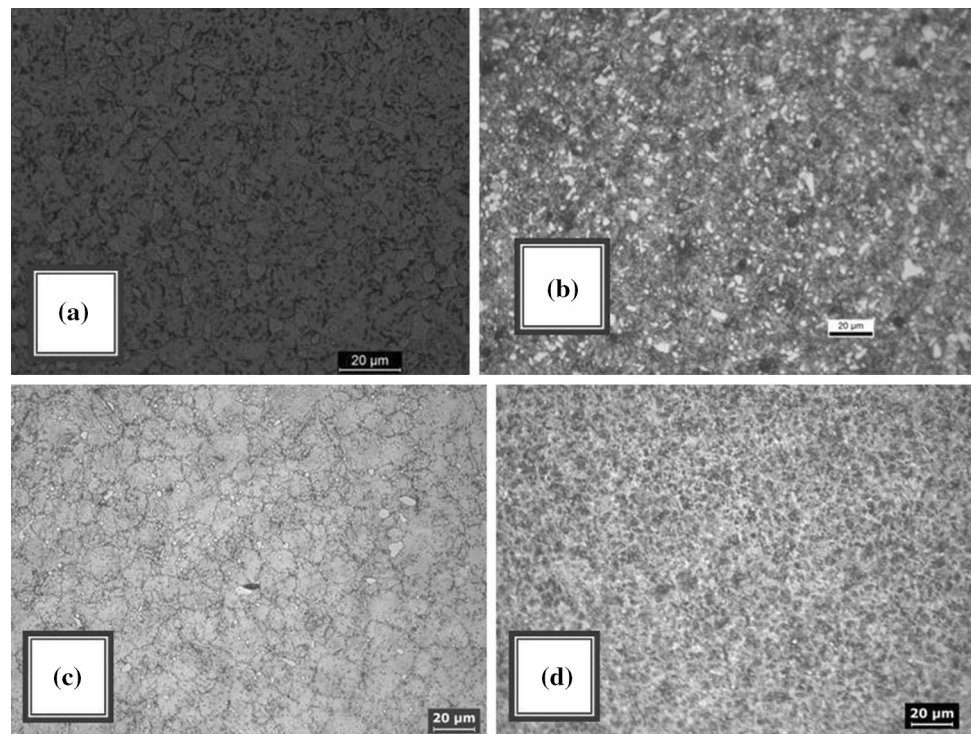


Table 1 Composition of various parts of bearing assembly B-1 and CMB-1

| Component | Base element | wt.% of elements | | | |
|--------------|--------------|------------------|------------|------------------|-------------|
| | | W | Cr | V | Mn |
| B-1 | | | | | |
| Ball | Fe | 8.7 ± 0.20 | 3.9 ± 0.10 | 1.2 ± 0.1 | 0.26 ± 0.01 |
| Outer race | Fe | 8.1 ± 0.20 | 3.4 ± 0.1 | 1.2 ± 0.2 | 0.23 ± 0.01 |
| Shaft | Fe | ... | 14.4 ± 0.1 | Cu = 0.18 ± 0.01 | |
| Cage | Cu | Al = 8.8 ± 0.2 | | | |
| CMB-1 | | | | | |
| Roller | Fe | 17.9 ± 0.30 | 4.4 ± 0.20 | 0.006 ± 0.0007 | 0.30 ± 0.01 |
| Outer race | Fe | 18.6 ± 0.30 | 3.9 ± 0.06 | 1.13 ± 0.01 | 0.31 ± 0.01 |
| Inner race | Fe | 18.3 ± 0.20 | 3.8 ± 0.04 | 1.12 ± 0.01 | 0.30 ± 0.01 |
| Cage | Fe | 0.10 ± 0.01 | 1.3 ± 0.02 | 0.98 ± 0.04 | 0.35 ± 0.06 |

of the assembly. Hardness of various parts was found to be constant across various regions, and the magnitude of hardness is consistent with expected value. Thus, failure due to metallurgical defects is ruled out.

Hardness of the races is generally maintained at similar levels or slightly lower than rollers in the bearing assembly. The inner surface of outer race of bearing B1 did not show the presence of any indentation. Failure due to ‘Brinelling’ or denting manifests with such indentation marks. High variation in the hardness values in the inner race and also little higher hardness of the inner race are also an indication of ‘Brinelling’ or denting, and such variation was also not observed. Thus, failure of the

bearing B-1 was certainly not due to ‘Brinelling.’ No untempered martensite, as evidenced by white etching layers, on the inner surface of the outer race or ball was noted indicating that the part was not locally heated to a very high temperature in service. Thus, failure due to overheating is also not the cause. However, it was observed that lubrication dried out completely. The failure of the bearing B-1 can be attributed to bulk damage to the bearing component outside contact zone. Such damages may have occurred as a result of one or more causes including overloading, bulk fatigue, permanent dimensional changes or misalignment due to operational problem. Strong evidence of failure due to misalignment was noted. This, in

turn, caused drying of lubrication and damage of bearing components due to excessive rubbing from resulting misalignment. At this stage, it is to be stated that the shaft and the outer race did not exhibit the presence of stress concentration. However, such stress concentration is expected, given the failure mechanism. This contrasting result can be attributed to the fact that the system was heated and was in heated condition for sufficiently long time to relieve the stresses. The temperature at which stress relieve occurred was considerably lower than overheating temperature at which tempering of martensitic structure takes place

Roughening and severe deformation of the outer surface of inner race and the presence of oxygen on the damaged

surface of cage also indicate that the component was subjected to higher temperature. The absence of lubrication and the dry-running condition have caused the generation of the higher temperature. In addition, there is metal contact between races and the rollers due to lack of lubrication of the bearing assembly as evident from stereo images, and this has contributed to the failure of the bearing due to undesirable heating and wear of various parts [14–16]. Most aero-engines are equipped with magnetic chip detector (MCD) which gives visual or audio signal at early stages of bearing wear or damages. Fighter aircraft moves with such high speed that even flying for short time after detection of metal chips may cause heavy damage of bearing systems.

Chemical analysis, microstructural studies and hardness suggested that the race and roller of CMB-1 nearly confirmed to high-speed tool steel T1 as per the ASTM specification and were used in the hardened and tempered conditions. Chemical analysis of the cage showed that it was made of 52,100 steel. The microstructure and the hardness suggested that the cage was used in the quenched

Table 2 Composition of various interstitial elements of various components of B-1 and CMB-1

| Component | wt.% of elements | |
|------------|------------------|---------------|
| | C | S |
| B-1 | | |
| Outer race | 0.76 ± 0.03 | 0.007 ± 0.001 |
| Balls | 0.82 ± 0.03 | 0.015 ± 0.004 |
| Cage | 0.13 ± 0.01 | 0.01 ± 0.001 |
| CMB-1 | | |
| Outer race | 0.75 ± 0.03 | 0.010 ± 0.007 |
| Inner race | 0.76 ± 0.04 | 0.014 ± 0.004 |
| Cylinder | 0.77 ± 0.03 | 0.008 ± 0.002 |
| Cage | 1.10 ± 0.09 | 0.007 ± 0.002 |

Table 5 Hardness of various components

| Component | B-1 | CMB-1 | CMB-2 | EDP-1 |
|--------------------------------------|----------|----------|----------|---------|
| Shaft/inner race/ stationary race | 310 ± 15 | 775 ± 35 | 700 ± 5 | 728 ± 5 |
| Outer race/rotating race | 710 ± 15 | 770 ± 25 | 700 ± 15 | 684 ± 8 |
| Cylinder/ball | 810 ± 20 | 777 ± 2 | 740 ± 10 | 764 ± 5 |
| Cage | 220 ± 5 | 256 ± 10 | 219 | 219 ± 2 |

Table 3 Composition of various parts of bearing assembly CMB-2

| Component | Base element | wt.% of elements | | | | |
|------------|--------------|------------------|-------------|-------------|---------|------|
| | | W | Cr | V | Cu | Al |
| Roller | Fe | 7.70 | 3.66 | 0.52 | ... | ... |
| Outer race | Fe | 8.52 ± 0.08 | 4.55 ± 0.22 | 1.70 ± 0.08 | – | ... |
| Inner race | Fe | 8.49 ± 0.08 | 4.35 ± 0.21 | 1.60 ± 0.08 | ... | ... |
| Cage | Cu | ... | ... | ... | Balance | 9.51 |

Table 4 Chemical composition of various components of EDP-1

| Component | Base element | wt.% of elements | | | | | | |
|------------------------------|--------------|------------------|---------------|---------------|----------|-------------|-------------|-----------|
| | | C | S | N | O | Cr | Mn | Al |
| Ball | Fe | 0.89 ± 0.020 | 0.010 ± 0.001 | 0.007 ± 0.002 | < 0.005 | 1.09 ± 0.02 | 0.22 ± 0.01 | |
| Stationary race (tight ring) | Fe | 0.97 | 0.011 | 0.034 | < 0.022 | 1.07 ± 0.02 | 0.22 ± 0.01 | ... |
| Rotating race (free ring) | Fe | 0.99 ± 0.020 | 0.010 ± 0.001 | 0.008 ± 0.002 | < 0.005 | 1.21 ± 0.02 | 0.22 ± 0.01 | ... |
| Cage | Cu | 0.02 | 0.014 | < 10 ppm | < 10 ppm | | | 8.2 ± 0.3 |

Fig. 6 Optical micrographs of the cages of (a) B-1, (b) CMB-1, (c) CMB-2 and (d) EDP-1

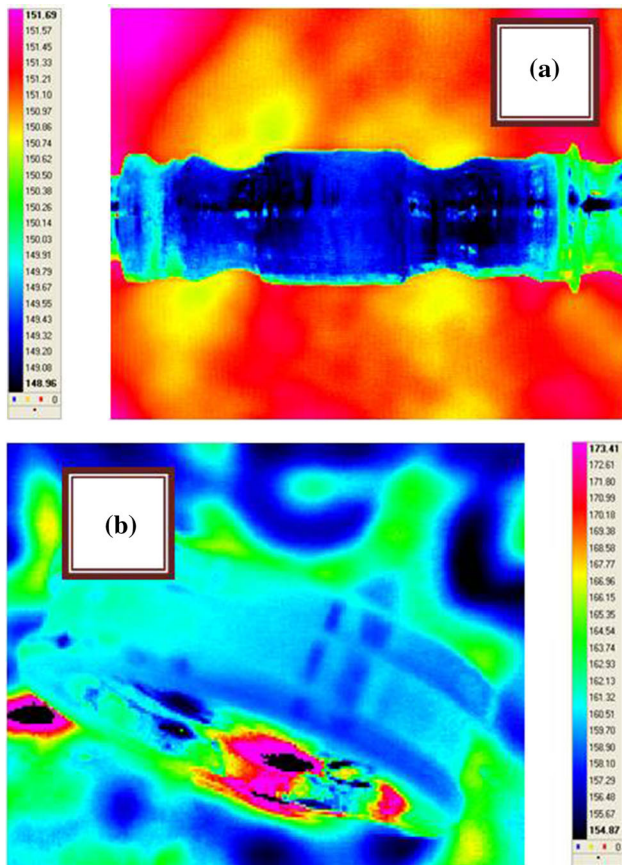
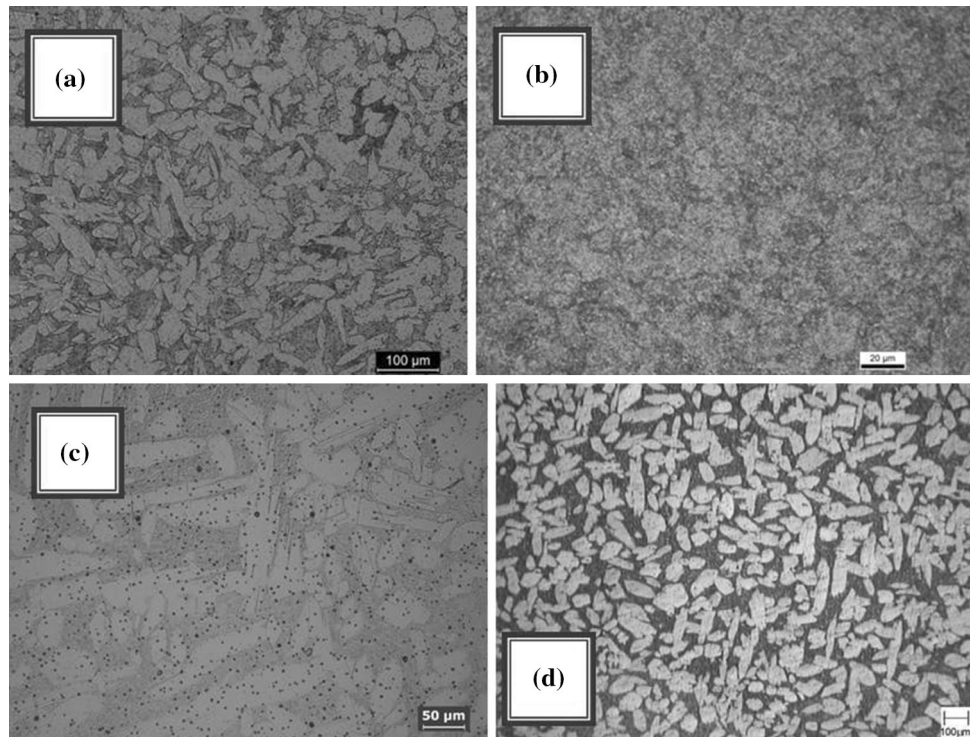


Fig. 7 Thermal imaging of the (a) shaft and the (b) outer race of bearing B-1 immediately after flash heating

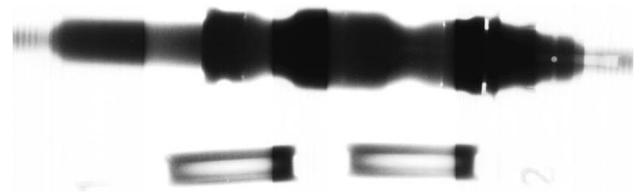


Fig. 8 Radiographic image of the shaft and the races

and tempered conditions. The microstructural features and the composition were uniform throughout various parts of the assembly. Hardness of various parts was found to vary considerably across various regions although the magnitude of hardness was consistent with expected value. Consistencies of the microstructure, composition and hardness in various locations of the failed components confirm failure is due to nonmetallurgical reason.

It was mentioned earlier that the hardness of the races is generally maintained at similar levels or slightly lower than rollers in the bearing assembly. The outer surface of inner race showed the presence of well-defined indentation spaced at a uniform pitch. Damage to a solid bearing surface characterized by one or more plastically formed indentations brought out by overload and is known as ‘Brinelling.’ High variation of hardness particularly hardness of races supports the possibility of ‘Brinelling.’ ‘Brinelling’ also occurs when indentations of the surface of a solid body due to repeated local impact or impacts or static overload. ‘Brinelling’ especially occurs in a roller-

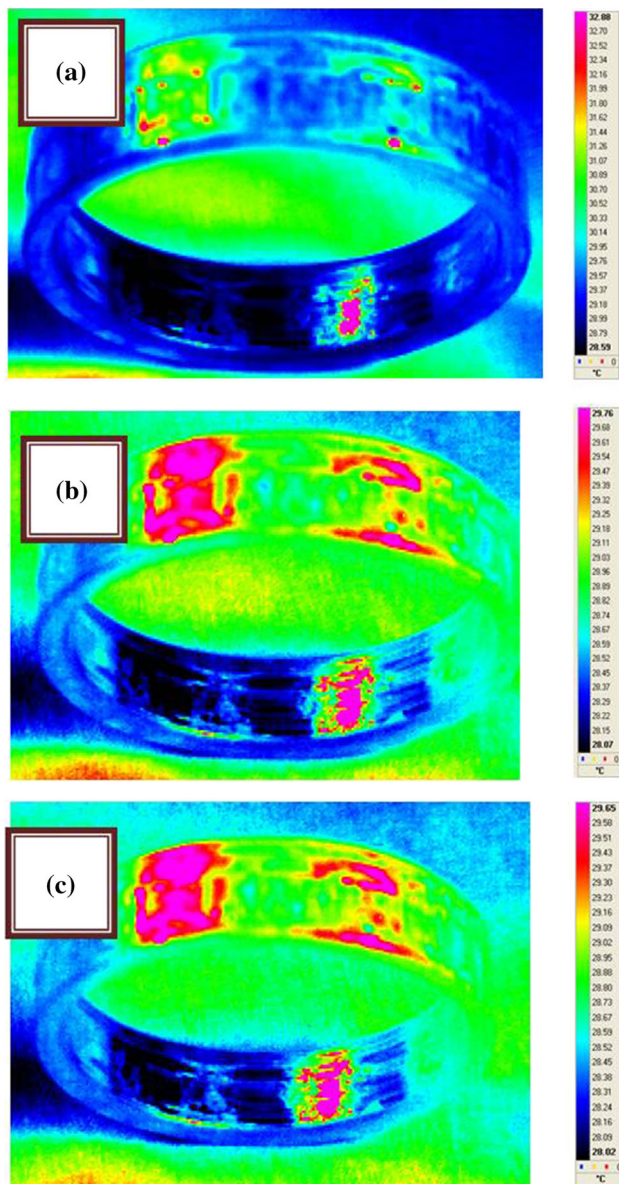


Fig. 9 Thermal images of the outer race of bearing CMB-1 (a) immediately after flash heating, (b) after 15 s and (c) after 30 s

bearing element. Failure due to ‘Brinelling’ or denting manifests with such indentation marks. ‘Brinelling’ is essentially an outcome of improper insertion of various parts of bearing assembly. Thus, it is to be noted that bearing system should be inserted by putting uniform pressure on the rings (races). It should not be inserted by putting pressure on the rollers. It is also pertinent to mention that this type of aircraft is primarily used for training purposes. The sealing of main shaft of these aircraft is made of labyrinth seals. Labyrinth seals contain series of knifelike, soft metal edges that ride very close to a steel surface. A certain amount of air, taken from the compressor, is forced between the steel surface and soft

metal edges to prevent oil leakage between sections. These seals are made of very soft metal and used at main bearing areas. Small nicks in the seal can cause major oil leaks and premature engine changes. It is also possible to have leakage of hot gases in this aircraft. The bearing temperature of this aircraft is controlled by determining the temperature of the engine oil. The oil consumption in this engine is 575 ml/h and maximum allowable temperature of oil is 120 °C and this is measured by E-type thermocouple.

Chemical analysis, microstructural studies and hardness indicated that the race and roller of CMB-2 bearing nearly confirmed to 8.5W–4.5Cr–1.5V–0.7C steel and were used in the hardened and tempered conditions. Chemical analysis of the cage showed that it was made of Cu–Al bronze. As expected, no metallurgical defects were noted across various locations.

There is a difference between the hardness of the core and the surface of the inner race, and this implies that the surface of inner race was subjected to high temperature, may be due to friction and then cooled rapidly by self-quenching. This resulted in the formation of untempered martensite. As mentioned earlier that the hardness of the races should generally be at similar levels or slightly higher than the rollers in bearings. The presence of untempered martensite, as evidenced by white etching layers, on the outer surface of the inner race indicated that the part was locally heated to a very high temperature in service. Blackening of various parts of the bearing, welding of the cage with the outer race and the presence of fully developed oxide scale on the damaged surface of inner race also indicate that the component was subjected to higher temperature. The absence of lubrication and the dry-running condition might have caused the generation of the higher temperature. In addition, there was evidence of metal-to-metal contact between races and the rollers due to lack of lubrication of the bearing assembly and transfer of material from the races to the cage [17–19] as observed with SEM examination. This resulted in formation of martensite by self-quenching from higher temperature, and this martensite was not tempered. The untempered martensite, being very hard and brittle, fractured during operation. These factors contributed to the failure of the bearing CMB-2 due to undesirable heating and wear of various parts.

The sealing of the main shaft of the helicopter is made of a kind of Russian coating designated as ‘KNA.’ There is no chance of leaking of hot gases through such sealing. Discoloring of the failed parts is due to formation of oxide scale and from the phase analysis of the oxide scale it is not possible to identify whether it is formed due to reaction with hot gases or due to generation of high temperature. Since transformation into martensite requires temperature in excess of 800 °C, it is unlikely that such high temperature can be as a result of leaking of high-pressure hot

Fig. 10 The SEM images showing morphology of worn surface of **a** outer race, **(b)** inner race, **(c)** rollers and **(d)** cages of CMB-2 along with EDS patterns

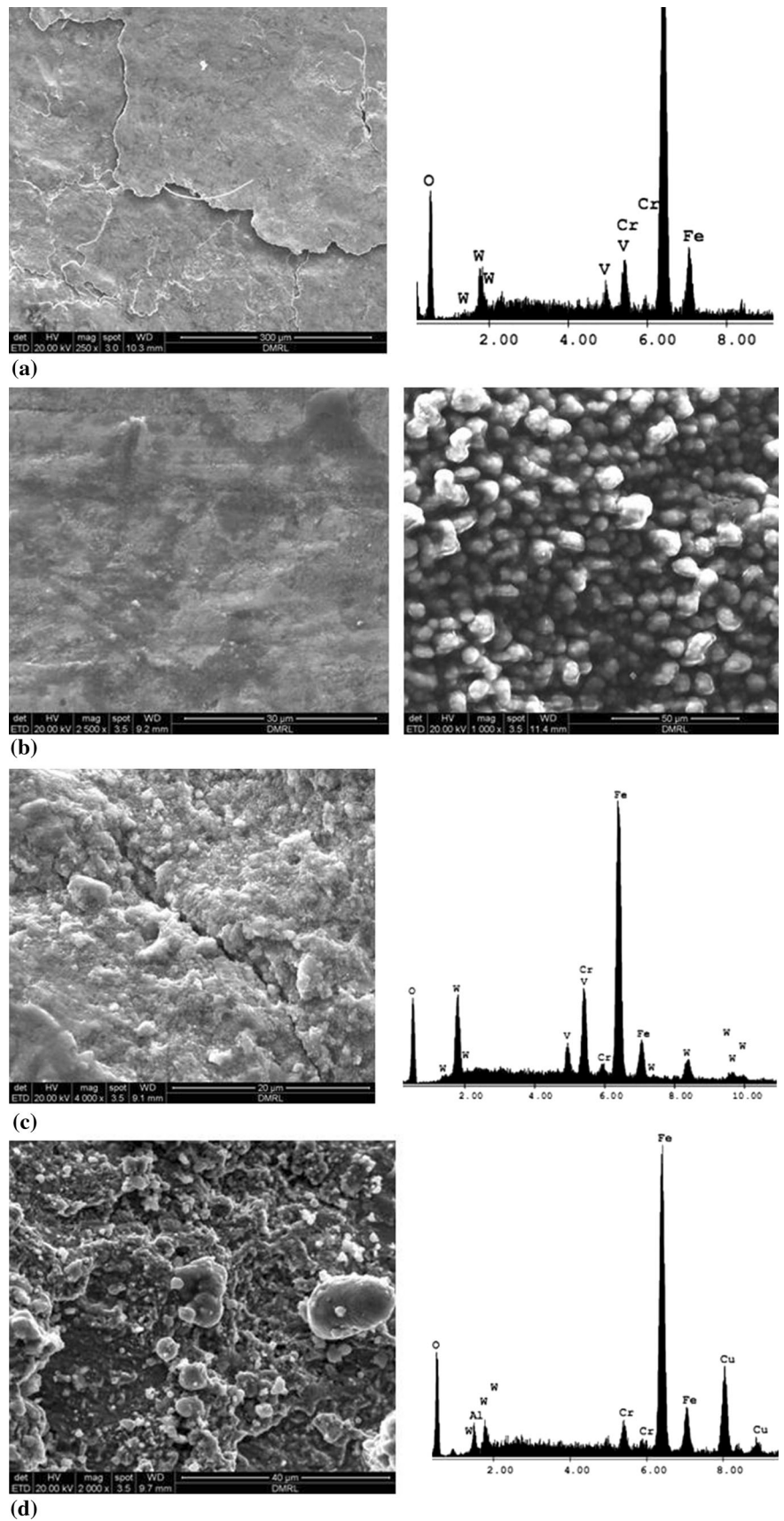
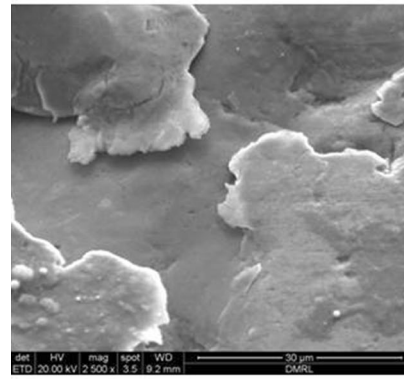
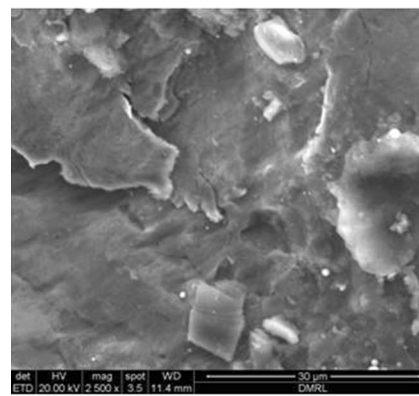
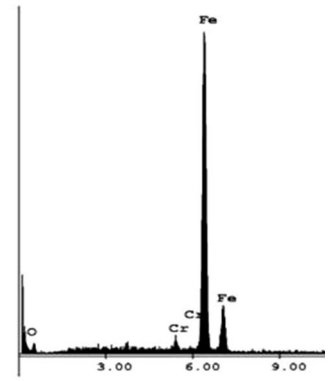


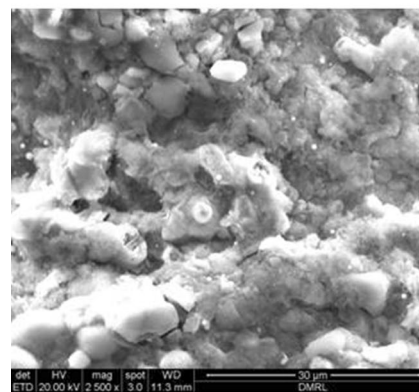
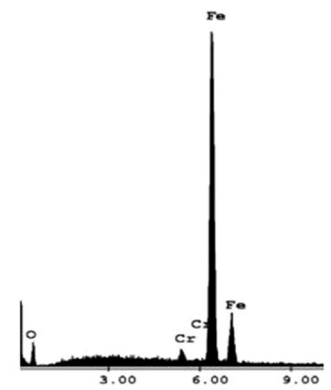
Fig. 11 SEM images of the damaged surfaces of **(a)** stationary race, **(b)** rotating race, **(c)** debris and **(d)** the ball along with EDS spectra of EDP-1 bearing



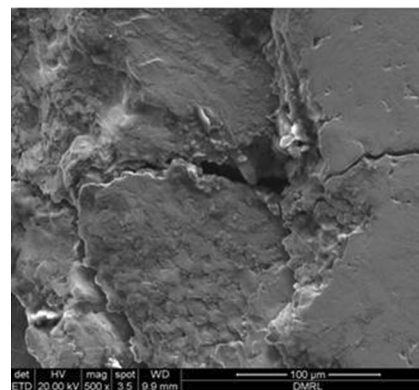
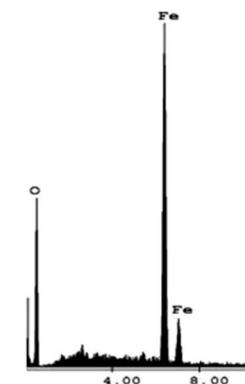
(a)



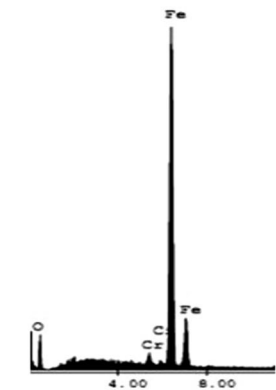
(b)



(c)



(d)



gases. The temperature of bearings of such engine is generally monitored by measuring the temperature of the oil. The maximum permissible oil temperature for this engine is 150 °C. The oil consumption rate is practically nil,

whereas the maximum permissible oil consumption limit is 0.3 l/h.

Analysis of chemistry, study of microstructure and hardness showed that the race and ball of EDP-1 bearing were fabricated by AISI 52,100 grade steel and were employed in the hardened and tempered conditions. The microstructure and chemical composition clearly resembled 52,100 steel. Chemical analysis of the cage indicated that it was made of Cu–Al alloy. However, the microstructure and the hardness suggested that the cage was used in cast condition.

Extensive plastic deformation of the damaged surfaces of stationary race (tight ring), rotating race (free ring) and ball and the presence of delamination/cracks in the region beneath the surfaces of these components clearly suggest

Table 6 Composition as obtained by EDS from damaged portion of various components

| Elements (wt.%) | Fe | Cr | Si | O |
|-----------------------------------|-------|------|------|-------|
| Stationary race (tight ring) | 96.81 | 1.75 | ... | 1.44 |
| Rotating race (free ring) | 95.4 | 1.90 | ... | 2.70 |
| Dirt of rotating race (free ring) | 84.07 | ... | 1.71 | 14.22 |
| Balls | 85.25 | 1.85 | ... | 3.30 |
| Dirt of balls | 83.90 | ... | ... | 16.10 |

Fig. 12 Optical image of the subsurface crack from the stationary race (tight ring)

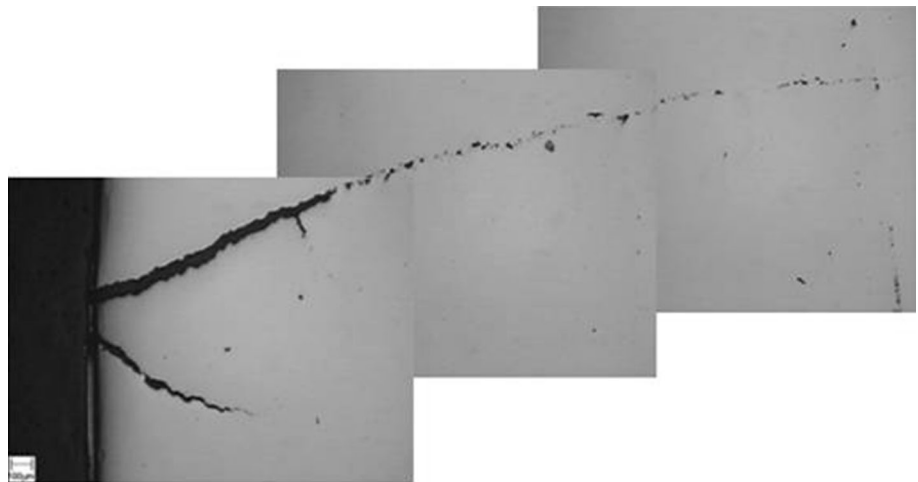
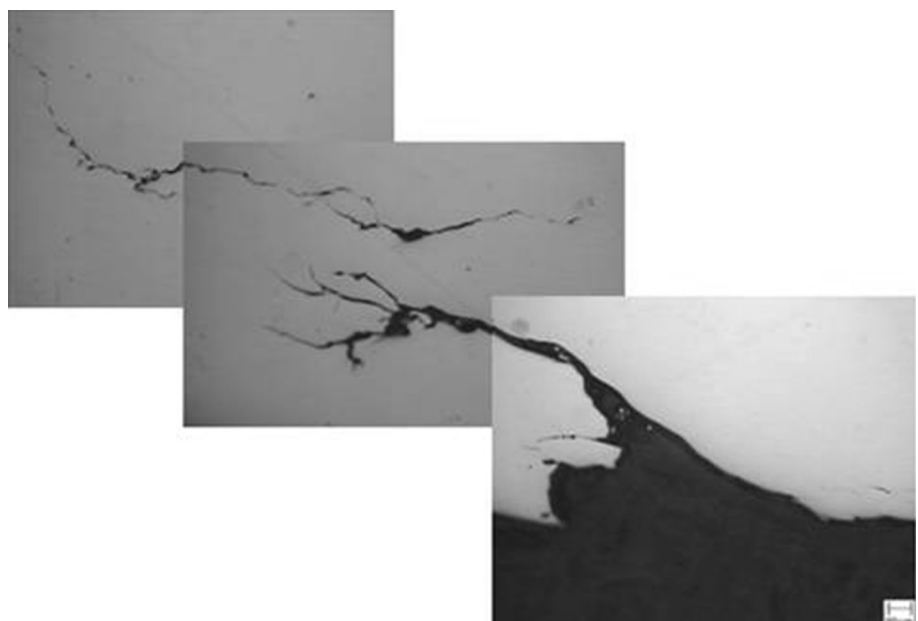


Fig. 13 Optical image of the subsurface crack of the ball



that all these components were subjected to delamination wear [20]. As significant amount of debris is noted on the damaged portion of rotating race (free ring) and balls, the wear is primarily due to abrasive action of the debris [21–23]. The debris may be ingested either during overhauling or generated during operation due to insufficient lubrication [24, 25]. The presence of foreign element on the damaged surface of the rotating race (free ring) confirms that some of the debris is due to foreign particles. Metallic debris can also be generated due to metal and metal contact as a result of insufficient lubrication. Insufficient lubrication has already been reported by preliminary visual inspection. All the debris was oxidized as temperatures were well above normal due to heat generated as a result of improper lubrication. The damaged surface of the balls exhibited vertical crack. These vertical cracks may be due to contact fatigue. Damaged surfaces of the balls did not show the presence of foreign element. Thus, the failure of balls could be due to abrasive action of oxidized metal debris generated by metal-to-metal contact and also by rolling contact fatigue [26, 27].

Finally, it is pertinent to discuss remedial measures to be taken in general. Presently, extensive research is going on for adapting intelligent bearing systems where a fully integrated self-powered wireless sensing system will be developed for future aircraft. Online condition monitoring can be achieved by the development of intelligent and integrated sensorized bearing called as ‘smart bearings’ consisting of miniaturized and low power consumption sensors, self-power ability for the operation of a wireless communication and data transfer. Smart bearings developed so far are primarily for automobile and railway industries with very limited availability for the harsh environment a jet engine experiences, such as high temperatures and vibration levels. Many methods are developed for online condition monitoring of the aero-engine bearing system [28–32]. This area, however, is outside my expertise. Additional measures to be taken are detailed in the text.

Additionally thin film thermocouple or thermal paints can be fixed on the stationary parts of the bearing system to measure and monitor the bearing temperature. Selection of commercial off-the-shelf sensors that are suitable for jet engine bearing operating conditions is very important. Vibration monitoring is an excellent and most widely used method for bearing condition monitoring. It gives diagnostic information that identifies defective components using bearing specific characteristic frequencies [33, 34]. Real-time monitoring of the load on the bearing can help understanding the dynamics of the engine under complex operating conditions. Monitoring the case speed will help in diagnosing problems associated with skidding, etc. Cage speed can be measured using non-contact methods such as

eddy current, capacitive sensors, magnetic, optical sensors, etc., and this in turn helps in enhancing bearing life. Last but not least, a disciplined approach with oil at all stages, use of correct grade oils with regular timely replacement and meticulous mounting practices of bearing will ensure enhanced bearing life.

Conclusions

1. Bearing B1 of cooling turbine of aircraft was damaged due to one or more causes including overloading, bulk fatigue, permanent dimensional changes or misalignment. This factor ultimately resulted in the cage broken; the balls were dislodged from the cage. Evidences of failure due to misalignment are conspicuous.
2. Center main bearing (CMB-1) of aero-engine was damaged due to ‘Brinelling’ or denting which manifested itself with indentation marks.
3. Bearing (CMB-2) of aero-engine failed due to lack of lubrication causing over heat and deformation of rollers by metal-to-metal contact. This factor ultimately resulted in formation of untampered martensite, leading to bearing failure.
4. Stationary race (tight ring) and rotating race (free ring) of bearing EDP-1 failed by delamination wear due to abrasive action of foreign particles and oxidized metallic particles generated due to metal to metal contact as a result of improper lubrication. Balls have failed by abrasive action of oxidized metal debris and may also be by rolling contact fatigue.

Acknowledgments The author is grateful to Director DMRL for giving permission to publish the paper. Author is grateful to the reviewer for his valuable suggestions.

References

1. P.J.L. Fernandes, Contact fatigue in rolling element bearing. *Eng. Fail. Anal.* **4**(2), 155–160 (1997)
2. J. Liua, H. Wua, Y. Shao, A theoretical study on vibrations of a ball bearing caused by a dent on the races. *Eng. Fail. Anal.* **83**, 220–229 (2008)
3. S.M. Muzakkir, H. Hirani, G.D. Thakre, M.R. Tyagi, Tribological failure analysis of journal bearings used in sugar mills. *Eng. Fail. Anal.* **18**, 2093–2103 (2011)
4. K.V. Sudhakar, J.C. Paredes, Failure mechanisms in motor bearings. *Eng. Fail. Anal.* **12**, 35–42 (2005)
5. R.K. Mishra, S.K. Muduli, K. Srinivasan, S.I. Ahmed, Failure analysis of an inter-shaft bearing of an aero gas turbine engine. *J. Fail. Anal. Prev.* **15**(2), 205–210 (2015)
6. N. Ejaz, I. Salam, A. Tauqir, Failure analysis of an aero engine ball bearing. *J. Fail. Anal. Prev.* **6**(6), 25–31 (2006)
7. R.R. Bhat, V. Nandi, V. Manohara, S.V. Suresh, Case study on failure of ball bearing of an aero-engine. *J. Fail. Anal. Prev.* **11**(6), 631–635 (2011)

8. Z.Q. Yu, Z.G. Yang, Failure analysis of fatigue fracture on the outer ring a cylindrical roller bearing in an air blower motor. *J. Fail. Anal. Prev.* **12**(4), 427–437 (2012)
9. M. Roy, M. Subramanian, G. Sundararajan, Room temperature erosion behaviour of a precipitation hardened stainless steel. *Tribol. Int.* **25**(4), 271–280 (1992)
10. J.D. Bressan, D.P. Baros, A. Sokolwski, R.A. Mesquita, C.A. Barbosa, Influence of hardness on the wear resistance of 17-4 PH stainless steel evaluated by the pin-on-disc testing. *J. Mater. Process. Technol.* **205**, 353–359 (2008)
11. P. Mukhopadhyay, P.S. Kannaki, M. Srinivas, M. Roy, Microstructural development during abrasive wear of M 50 bearing steel. *Wear* **315**, 31–37 (2014)
12. M. Roy, A. Pauschitz, J. Wernisch, F. Franek, Influence of mating surface on elevated temperature wear of 253 MA alloy. *Mater. Corros.* **55**, 259–273 (2004)
13. N. Saka, A.M. Eleiche, N.P. Suh, Wear of metals at high sliding speed. *Wear* **44**, 109–125 (1977)
14. F.H. Stott, High temperature sliding wear of metals. *Tribol. Int.* **35**, 489–495 (2002)
15. M. Roy, K.K. Roy, G. Sundararajan, Erosion–oxidation interaction in Ni and Ni-20Cr alloy. *Metall. Mater. Trans.* **32A**, 1431–1451 (2001)
16. R. Büscher, B. Gleising, W. Dudzinski, A. Fischer, The effects of subsurface deformation on the sliding wear behaviour of a microtextured high-nitrogen steel surface. *Wear* **257**, 284–291 (2004)
17. M. Roy, A. Pauschitz, F. Franek, Comparative evaluation of ambient temperature friction behaviour of thermal sprayed Cr₃C₂-25(Ni20Cr) Coating with conventional and nanocrystalline grains. *Tribol. Int.* **39**, 29–38 (2006)
18. K.R. Lawless, in *Interdisciplinary Approach to Friction and Wear*, ed. by P.M. Ku (NASA SP-181, 1968), p. 433
19. R.K.J. Wood, M. Roy, Tribology of thermal sprayed coatings, in *Surface Engineering for Enhanced Performance against Wear*, ed. by M. Roy (Springer, Vienna, 2013), pp. 1–43
20. N.P. Suh, An overview of the delamination theory of wear. *Wear* **44**, 1–16 (1977)
21. M. Roy, C.V. Subba Rao, D. Srinivas Rao, G. Sundararajan, Abrasive wear behaviour of detonation sprayed WC–Co coatings on mild steel. *Surf. Eng.* **15**, 129–136 (1999)
22. I. Garbar, Abrasion resistance as a function of substructural changes in steel. *Wear* **258**, 275–280 (2005)
23. S. Sarkar, E. Badisch, R. Mitra, M. Roy, Impact abrasive wear response of carbon/carbon composites at elevated temperatures. *Tribol. Lett.* **37**, 445–451 (2010)
24. M. Roy, Y. Tirupataiah, G. Sundararajan, Effect of particle shape on the erosion of cu and its alloys. *Mater. Sci. Eng., A* **165**, 51–63 (1993)
25. K. Kusumoto, K. Shimizu, X. Yaer, H. Hara, K. Tamura, H. Kawaia, High erosion–oxidation performance of Fe-based Nb or V containing multi-component alloys with Co addition at 1173 K. *Mater. Des.* **88**, 366–374 (2015)
26. M. Roy, Wear testing: an assessment of test methodology. *Trans. Indian Inst. Met.* **53**(6), 623–638 (2000)
27. Yuji Ohue, Koji Matsumoto, Sliding–rolling contact fatigue and wear of maraging steel roller with ion-nitriding and fine particle shot-peening. *Wear* **263**, 782–789 (2007)
28. Z. Zhao, Z. Liu, Y. Lu, J. Hu, Numerical modelling of unsteady oil film motion characteristics in bearing chambers. *Int. J. Turbo Jet-Engines* **32**(3), 233–245 (2015)
29. J. Mihalčová, State of aircraft turboshaft engines by means of tribotechnical diagnostic. *Int. J. Turbo Jet-Engines* **35**(1), 11–16 (2018)
30. Mariusz Żokowski, Paweł Majewski, Jarosław Spychała, Detection damage in bearing system of jet engine using the vibroacoustic method. *Acta Mech. Autom.* **11**(3), 237–242 (2017)
31. N. Tandon, A. Choudhury, A review of vibration and acoustic measurement methods for the detection of defects in rolling element bearings. *Tribol. Int.* **32**, 469–480 (1999)
32. P.D. McFadden, J.D. Smith, Vibration monitoring of rolling element bearings by the high-frequency resonance technique—a review. *Tribol. Int.* **17**, 3–10 (1984)
33. R.B. Randall, J. Antoni, Rolling element bearing diagnostics—a tutorial. *Mech. Syst. Signal Process.* **25**, 485–520 (2011)
34. M.S. Patil, J. Mathew, P.K.R. Kumar, Bearing signature analysis as a medium for fault detection: a review. *J. Tribol.* **130**, 14001 (2008)

Publisher's Note Springer Nature remains neutral with regard to jurisdictional claims in published maps and institutional affiliations.